Selective Decoupling and Hamiltonian Engineering in Dipolar Spin Networks

A. Ajoy, U. Bissbort, D. Poletti, and P. Cappellaro

Phys. Rev. Lett. **122**, 013205 — Published 10 January 2019

DOI: 10.1103/PhysRevLett.122.013205

Selective decoupling and Hamiltonian engineering in dipolar spin networks

A. Ajoy,[1,*] U. Bissbort,[2,3,*] D. Poletti,[3] and P. Cappellaro[2]

[1] *Department of Chemistry, University of California Berkeley, and Materials Science Division Lawrence Berkeley National Laboratory, Berkeley CA*[†]

[2] *Research Laboratory of Electronics and Department of Nuclear Science & Engineering, Massachusetts Institute of Technology, Cambridge, MA*

[3] *Science and Math Cluster and EPD Pillar, Singapore University of Technology and Design, 8 Somapah Road, 487372 Singapore*

We present a protocol to selectively decouple, recouple, and engineer effective interactions in mesoscopic dipolar spin networks. In particular, we develop a versatile protocol that relies upon magic angle spinning to perform Hamiltonian engineering. By using global control fields in conjunction with a local actuator, such as a diamond Nitrogen Vacancy center located in the vicinity of a nuclear spin network, both global and local control over the effective couplings can be achieved. We show that the resulting effective Hamiltonian can be well understood within a simple, intuitive geometric picture, and corroborate its validity by performing exact numerical simulations in few-body systems. Applications of our method are in the emerging fields of two-dimensional room temperature quantum simulators in diamond platforms, as well as in molecular magnet systems.

PACS numbers: 03.67.Ac, 76.60.-k, 03.67.Lx

The concept of Hamiltonian engineering has widespread applications in quantum information processing [1–4], quantum metrology [5], and in the challenge of constructing suitable platforms for quantum simulation, both analog and digital [6–9]. In essence, it consists in performing operations on a naturally occurring system to give rise to an effective Hamiltonian, which is of fundamental interest or of direct use for the task at hand [10–12]. Numerous quantum control techniques developed over several decades, originating from the field of nuclear magnetic resonance (NMR), have been employed as Hamiltonian engineering tools. For instance, they have been used to effectively cancel ("decouple") interactions, thereby isolating a quantum system from its environment and greatly increasing coherence times [13].

A technique with extensive application in NMR systems to tune dipolar couplings by exploiting its symmetry properties is magic angle spinning (MAS), which traditionally comes in two variants: (i) magic angle spinning in physical space [14], where the solid sample is spatially rotated at high frequency around an axis tilted at the magic angle $\theta_M = \arctan\sqrt{2} \approx 54.7^\circ$ relative to a large static external magnetic field $\mathbf{B}_0$; (ii) MAS in spin space – achieved either by continuous off-resonant RF irradiation (Lee-Goldberg decoupling [15, 16]) or by a successive application of discrete rotation pulses (*tetrahedral* averaging [17, 18].)

The goal of this work is to extend MAS to nanoscale and mesoscopic systems in order to *engineer* (decouple and recouple) the Hamiltonian of dipolar coupled spin networks [21]. The key ingredients of our method are: (i) a bang-bang control construction [22], toggling between two piecewise constant magnetic fields $\mathbf{B}_0$ and $\mathbf{B}_1$, that can amplify the effects of even a small transverse magnetic field and achieve a spin rotation around the magic angle θ_M for fractions $2\pi/m$; (ii) a spin actuator [23–25] that introduces the transverse magnetic field only locally, thus implementing the rotation construction at the nanoscale. While the technique is more generally applicable to a variety of different experimental realizations, including molecular magnet qubit systems comprised of inorganic complexes such as vanadium(IV) [26–29], for clarity here we focus on a specific system comprising a shallow Nitrogen Vacancy (NV) center in diamond [19, 24, 30–32] coupled to a nuclear spin network on the surface above it (Fig. 1 (a)) [20, 33, 34]. These systems have emerged as a promising platform for quantum simulation at room temperature [19, 35, 36], and for probing localization and critical phenomena in strongly interacting 2D systems [20, 37]. Given the small length scales of these quantum networks, they have been traditionally considered hard to control, even with ultrastrong magnetic gradients [38, 39]. Instead, as we shall show here, a local actuator up to 10nm away, combined with our new generation of MAS techniques, provides a viable and simple means to engineer these networks at the nanoscale and obtain selective decoupling by four orders of magnitude.

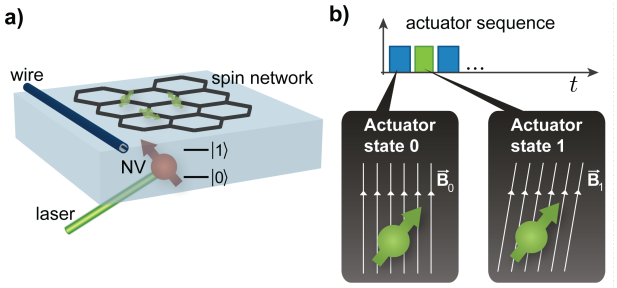

FIG. 1. **Actuator based selective decoupling and recoupling in spin networks:** (a) A NV center a few nanometers below the diamond surface, optically initialized and controlled by microwave irradiation, interacts with a spin network (eg. fluorographene [19] or hBN [20]). (b) By toggling the NV center between the $|m = 0\rangle$ and $|m = -1\rangle$ states, the effective (hyperfine) field for the spin network can be turned on and off, realizing two different, discrete Hamiltonians employed to engineer the effective interaction.

We first provide an intuitive, geometric picture of MAS for a pair of spins. Describing spin j with the vectorial spin operator $\mathbf{I}^{(j)} = [I_x^{(j)}, I_y^{(j)}, I_z^{(j)}]$, any two spins j and j' at positions $\mathbf{r}_j$ and $\mathbf{r}_{j'}$ interact via the dipolar Hamiltonian $\mathcal{H}_{j,j'} = D_{j,j'}(3(\mathbf{I}^{(j)} \cdot \mathbf{e}_{jj'})(\mathbf{I}^{(j')} \cdot \mathbf{e}_{jj'}) - \mathbf{I}^{(j)} \cdot \mathbf{I}^{(j')})$,

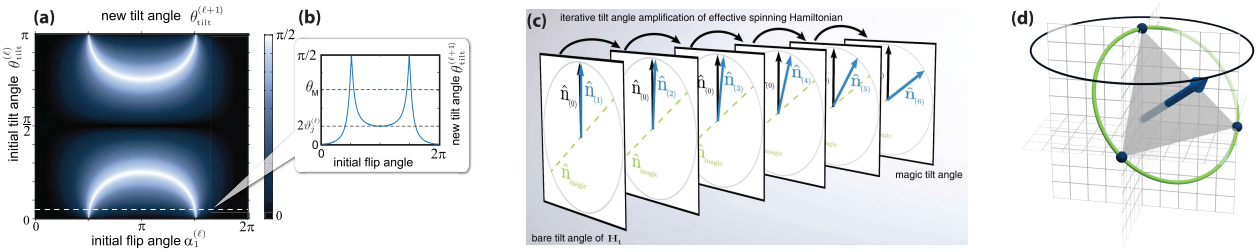

FIG. 2. **Actuator control of spin network:** Tilt angle $\theta_{\rm tilt}^{(l+1)}$ after a single iteration of the protocol at a small initial tilt angle $\theta_{\rm tilt} = \pi/10$ is shown in (a) and (b). The regimes of high sensitivity [i.e. large slope in (b)] are reflected by the large white arc, with the strong dependence on $\theta_{\rm tilt}^{(l)}$ enabling spatial selectivity in the vicinity of an actuator. Iteration of the protocol, shown in (c), leads to exponential amplification of the effective tilt angle with the blue arrow depicting the effective rotation axis in the respective step. (d) Geometric picture of the decoupling to lowest Magnus order: the effective vectorial parts of the secular Hamiltonian (blue spheres) are successively rotated around the magic angle axis (blue diagonal arrow), leading to a cancellation of terms.

with $D_{j,j'} = -\mu_0\gamma_j\gamma_{j'}/(8\pi r_{j,j'}^3)$, where γ_j is the gyromagnetic ratio of particle j, $r_{j,j'} = |\mathbf{r}_j - \mathbf{r}_{j'}|$ is the distance and $\mathbf{e}_{jj'} = (\mathbf{r}_j - \mathbf{r}_{j'})/r_{j,j'}$ and we set $\hbar = 1$. This interaction form applies to both the pairwise interaction between any two spins, as to the NV-spin interaction with the NV's gyromagnetic ratio γ_e being that of the electron. In the secular approximation[40], this reduces to $\mathcal{H}_{1,2}^{(\rm sec)} \propto [3I_z^{(1)}I_z^{(2)} - \mathbf{I}^{(1)}\cdot\mathbf{I}^{(2)}]$.

We associate a 3D vector $\mathbf{v}$ with any two-spin operator $\sum_{d\in\{x,y,z\}} v_d I_d^{(1)} I_d^{(2)}$. For example, the scalar operator term $\mathbf{I}^{(1)}\cdot\mathbf{I}^{(2)}$ in $\mathcal{H}_{1,2}^{(\rm sec)}$ corresponds to a vector lying at the magic angle $\theta_{\rm M}$ (blue arrow in Fig. 2(d)). The first term $I_z^1 I_z^2$ lies on the z-axis and, as shown in Fig. 2(d) as blue spheres, it is successively rotated on the green circle around the rotation axis at $\theta_{\rm M}$, such that the average of its positions (here for $L = 3$ steps) lies on the magic axis. This average exactly cancels out the scalar vector contribution, thus geometrically demonstrating decoupling to lowest order. The Hamiltonian rotation needed for decoupling can be achieved via a multi-pulse sequence. Each spin is exposed to the same ideal (instantaneous) pulse $\mathcal{U}_{\rm rot} = e^{-i\alpha H_{\mathbf{n}}}$, rotating the spin around an axis $\mathbf{n}$ by an angle $\alpha = 2\pi/L$ with $L \in \mathbb{N}$. To decouple the two spins, we consider a long sequence of evolutions under $\mathcal{H}_{1,2}$ for time τ, interrupted by rotations $\mathcal{U}_{\rm rot}$. For a subset of L such operations, the total evolution operator $\mathcal{U}_{\rm tot} = \left[e^{-i\alpha H_{\mathbf{n}}} e^{-i\tau\mathcal{H}_{1,2}}\right]^L$ can be exactly rewritten as $\mathcal{U}_{\rm tot} = \mathcal{G}_1\mathcal{G}_2\ldots\mathcal{G}_L$ with $\mathcal{G}_m = \mathcal{U}_{\rm rot}^m e^{-i\tau\mathcal{H}_{1,2}}\mathcal{U}_{\rm rot}^{\dagger m}$, where we iteratively inserted $\mathcal{U}_{\rm rot}^m\mathcal{U}_{\rm rot}^{\dagger m} = \mathbb{1}$. Pulling the increasing rotation operators into the exponential, $\mathcal{G}_m = e^{-i\tau\mathcal{U}_{\rm rot}^m\mathcal{H}_{1,2}\mathcal{U}_{\rm rot}^{\dagger m}}$, we can geometrically interpret $\mathcal{U}_{\rm tot}$ as the evolution under piecewise constant, successively rotated dipolar Hamiltonians. Setting $\mathbf{n}$ such that $\mathcal{G}_m$ rotates around the magic axis, achieves decoupling. Mathematically, the evolution under $\mathcal{U}_{\rm tot}$ is described in a Magnus expansion and well approximated by its lowest order, the average Hamiltonian $\overline{\mathcal{H}}_{j,j'}^{(\rm sec),0} = \sum_{m=0}^{L-1}\mathcal{U}_{\rm rot}^m\mathcal{H}_{j,j'}\mathcal{U}_{\rm rot}^{\dagger m}$.

In typical experiments, the magnitude of $\mathbf{B}_0$ makes a direct generation of a rotation $\mathcal{U}_{\rm rot} = e^{-i\alpha H_{\mathbf{n}}}$ with $\mathbf{n}$ at the magic angle infeasible. It is this limitation that our protocol mitigates, by achieving the desired rotation axis with an iterative construction. The required basic ingredients are two single-spin Hamiltonians $\mathcal{H}_{0/1}^{(j)} = \gamma_I\mathbf{B}_{0/1}^{(j)}\cdot\mathbf{I}^{(j)}$ (possibly depending on spin j), which are created by magnetic fields $\mathbf{B}_{0/1}^{(j)}$ with a small relative tilt. $\mathbf{B}_0$ is a global, uniform, static background field, while $\mathbf{B}_1^{(j)}$ contains, in addition to $\mathbf{B}_0$, a current-induced contribution from a nearby wire. We also envision using a nearby NV center as a local actuator for the spins: toggling between two NV internal states $|m=0\rangle$ and $|m=-1\rangle$ creates an additional spin-specific contribution to the field. The toggling between $\mathcal{H}_0$ and $\mathcal{H}_1$ occurs by synchronously flipping the NV state and sending piecewise constant pulses of current through the wire.

We shall now describe the construction of the effective rotation operator, by iteratively amplifying the tilt angle $\theta := \sphericalangle(\mathbf{B}_0, \mathbf{B}_1)$ as shown in Fig. 2(c), ultimately allowing the magic angle to be reached. As the elementary building block of our procedure, we let the spin evolve under piecewise constant $\mathcal{H}_1$, $\mathcal{H}_0$ and $\mathcal{H}_1$ for times τ_1, τ_0 and τ_1 respectively, as shown in Fig. 1(b). Our aim, as detailed below, will be to rotate the spins close to the magic angle. Omitting the spin label, the evolution of a single spin[41] is thus described by the elementary propagator $\mathcal{U}_{\rm el} := \mathcal{R}(\alpha_1, \hat{\mathbf{n}}_1)\,\mathcal{R}(\alpha_0, \hat{\mathbf{n}}_0)\,\mathcal{R}(\alpha_1, \hat{\mathbf{n}}_1)$, where $\mathcal{R}(\alpha, \hat{\mathbf{n}}) := e^{-i\alpha\mathbf{I}\cdot\hat{\mathbf{n}}}$ is the rotation operator around the axis $\hat{\mathbf{n}}$ by the flip angle α, and the bare tilt angle of $\hat{\mathbf{n}}$ is $\theta_{\rm tilt}^{(0)} = \mathrm{atan}(\hat{\mathbf{n}}\cdot\mathbf{e}_z)$. Being a sequence of rotations, $\mathcal{U}_{\rm el} = e^{i\phi_{\rm el}}\mathcal{R}(\alpha_{\rm el}, \hat{\mathbf{n}}_{\rm el})$ is nothing but a rotation operator itself, up to an unimportant phase $\phi_{\rm el}$. The functional dependence of the effective axis $\mathbf{n}_{\rm el}$ and flip angle $\alpha_{\rm el}$ on the elementary parameters can be worked out analytically [42]. Let us summarize the main results: the effective rotation axis and flip angle are $\mathbf{n}_{\rm el} = 2b\sin\frac{\alpha_1}{2}\hat{\mathbf{n}}_1 + \sin\frac{\alpha_0}{2}\hat{\mathbf{n}}_0$ and $\alpha_{\rm el} = 2\arccos\left(\left|2b\cos\frac{\alpha_1}{2} - \cos\frac{\alpha_0}{2}\right|\right)$ respectively, where $b = \cos\frac{\alpha_0}{2}\cos\frac{\alpha_1}{2} - (\hat{\mathbf{n}}_0\cdot\hat{\mathbf{n}}_1)\sin\frac{\alpha_0}{2}\sin\frac{\alpha_1}{2}$. Importantly, the rotation axis associated with $\mathcal{U}_{\rm el} = e^{-i\overline{\mathcal{H}}}$ and the effective Hamiltonian $\overline{\mathcal{H}}$ lie in the plane spanned by the rotation axes $\mathbf{n}_0$ and $\mathbf{n}_1$ of the original Hamiltonians, i.e. only the tilt angle is changed and possibly amplified [42, 43]. In this work, we generally fix $\alpha_0 = \pi$ and neglect spin decoherence for simplicity. For the case $\alpha_1 = \pi$, one finds that the tilt angle is exactly doubled by this protocol. The dependence of the tilt and flip angle of the effective elementary rotation on α_1 (see Fig. 2) shows distinct regimes of *high* and *low sensi-*

tivity on the initial tilt angle [corresponding to steep and shallow slopes in Fig. 2(b)]. For any initial tilt angle $0 < \theta_{\rm tilt}^{(0)} \lesssim \pi/4$ (typical for experiments), the effective tilt angle can actually reach the magic angle with only one application of $\mathcal{U}_{\rm el}$, but at the cost of a very small flip angle [close to 0 or 2π in Fig. 2(a) and (b)]. Alternatively, by concatenating the procedure $\mathcal{U}^{(k)} \mapsto \mathcal{U}^{(k+1)} = \mathcal{U}^{(k)}\mathcal{R}(\alpha_0, \hat{\mathbf{n}}_0)\mathcal{U}^{(k)}$ with the initial $\mathcal{U}^{(1)} = \mathcal{R}(\alpha_1, \hat{\mathbf{n}}_1)$, one can amplify the tilt angle, exponentially in the number of concatenations (e.g. doubling $\theta_{\rm tilt}^{(l)}$ at $\alpha_1 = \pi$ with every iteration). Given a small initial bare tilt angle of $\mathbf{B}_1$ (we use $\theta_{\rm tilt}^{(0)} = 1.432°$ throughout this work, well within reach for typical nuclear spin systems [19, 32]), a general iteration of the elementary concatenation $\mathcal{U}^{(N_c)}$ (e.g. for $\alpha_1 = \pi$) does generally not exactly lead to the magic angle unless $2^{N_c}\theta_{\rm tilt}^{(0)} = \theta_{\rm M}$. We therefore introduce a control sequence that gives our final protocol, reaching the desired total unitary [44]

$$\mathcal{U}_{\rm tot} = \mathcal{U}^{(N_c)}e^{-i\tau_b\mathcal{H}_0}\mathcal{U}^{(N_c)}e^{-i\tau_a\mathcal{H}_0}\mathcal{U}^{(N_c)}e^{-i\tau_b\mathcal{H}_0}\mathcal{U}^{(N_c)}. \quad (1)$$

The point (τ_a, τ_b), which optimizes the sequence, is generally not unique and different points feature different decoupling characteristics and *sensitivity* (i.e. the strength of the effective tilt angle dependence on α_1), a feature that allows for further tuning of the effective interactions. The total time required by $\mathcal{U}_{\rm tot}$ is $\tau_{\rm rot} = \tau_a + 2\tau_b + 4[2^{N_c}\tau_1 + (2^{N_c}-1)\tau_0]$, which, in contrast to the usual idealized discrete rotation pulses used in MAS [17], may be non-negligible on the time scale of the inverse dipolar interactions. To perform decoupling, we let the system evolve freely under $\mathcal{H}_0$ for a wait time τ between the rotations $\mathcal{U}_{\rm tot}$.

Effective Hamiltonian: For the interaction to be efficiently canceled, we need to consider m repetitions of the rotation by $2\pi/m$. The Hamiltonian is then periodic with period $\tau_{\rm rot} + \tau$ and the evolution of any state can be described within average Hamiltonian theory [45] when evaluated stroboscopically. To quantitatively evaluate the decoupling effects on the spin dipolar couplings, we consider the effective (Floquet) Hamiltonian over a period $T = m(\tau_{\rm rot} + \tau)$ in the toggling frame [45], $\overline{\mathcal{H}}_I = \frac{i}{T}\ln[\mathcal{U}_I(t_0, t_0+T)]$ (technical details in [42]). $\overline{\mathcal{H}}_I$ can be decomposed into a series of terms: scalar, single-spin and two-spin interactions. Since we aim at engineering or canceling a two-spin interaction Hamiltonian, we focus on the two-spin terms, arising from the averaging of the spin network dipolar Hamiltonian. This can be extracted by projecting $\overline{\mathcal{H}}_I$ on the subset of two-spin operators, leading to the operator expansion coefficients $h_{k,l}^{(j,j')} = {\rm Tr}\left[\overline{\mathcal{H}}_I(\sigma_k^{(j)} \otimes \sigma_l^{(j')})\right]/4$. To quantify the effective coupling strength, we use the Frobenius norm $\overline{\mathcal{S}}_{j,j'} = \|\overline{\mathcal{H}}_{j,j'}\|_F$ of the associated operator $\overline{\mathcal{H}}_{j,j'} = \sum_{k,l} h_{k,l}^{(j,j')}\sigma_k \otimes \sigma_l$ on the two-spin space [42]. The bare interaction strength $\mathcal{S}_{j,j'}$ can be quantified analogously and we thus define the decoupling ratio $\mathcal{R}_{j,j'} = \overline{\mathcal{S}}_{j,j'}/\mathcal{S}_{j,j'}$.

Hamiltonian Engineering: To demonstrate our protocol, we first consider decoupling and local recoupling of a nuclear ^{13}C spin pair, located at positions $\mathbf{R}_{1/2} = [x_{1/2}, 0, 0]^t$ (Fig. 3(a)), where our method reaches high decoupling efficacy. Starting in a low sensitivity regime at $\tau_1 = \pi/|\mathbf{B}_0|$, $N_c = 5$ and $m = 3$, we numerically optimize the decoupling with respect to (τ_a, τ_b, τ) (in the absence of the NVs) by initializing the minimization close to the half integer decoupling peak at $\tau = 1000.5 \times 2\pi/(\gamma_{\rm I}|\mathbf{B}_0|)$. Using these optimized parameters, we show the resulting interaction strength $\|\overline{\mathcal{H}}_{j,j'}\|_F$ and decoupling ratio $\mathcal{R}_{j,j'}$ in Fig. 3(b) and (c) respectively. Interestingly, if the spins are farther apart than ≈ 0.2nm, $\mathcal{R}_{j,j'}$ converges to a constant, i.e. becomes distance independent and isotropic. This also holds for parameters away from high decoupling. Decoupling by three to four orders of magnitude is reached in Fig. 3 [46], a non-trivial result given the highly non-ideal nature of the pulses compared to the typical assumptions of instantaneous pulses (comparison in [42]) entering the intuitive explanation of MAS. The high efficacy of the decoupling is corroborated by the strongly suppressed growth of the entanglement entropy of two spins initially prepared in the uncorrelated state $|\uparrow\rangle \otimes |\downarrow\rangle$, shown in Fig. 3(d) as orange dots, as compared to the same system without the protocol (black dots).

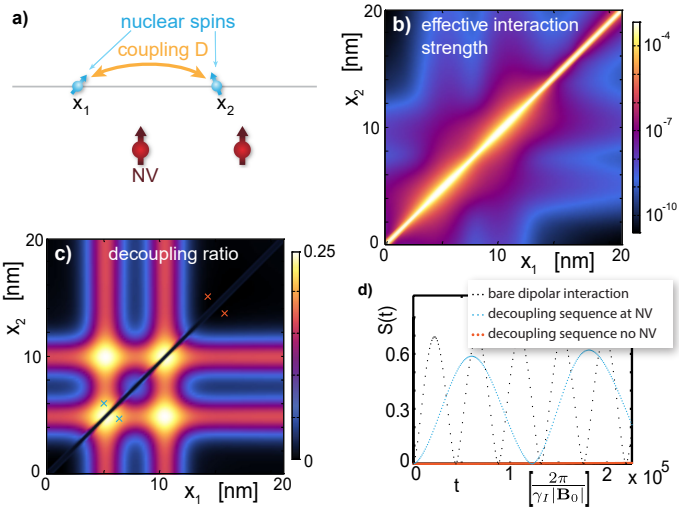

FIG. 3. **Decoupling and selective recoupling via local actuators:** By locally disturbing the optimal decoupling field strength using 2 NV centers (as sketched in (a)), the electronic state of which can be toggled in synchrony with the $\mathbf{B}_1$ magnetic field, the effective interaction between two nuclear spins can be made spatially dependent. Furthermore, the *disturbance* of the perfect decoupling is essentially additive in contribution from both NVs. This is reflected by both the effective interaction strength $\overline{\mathcal{S}}_{1,2}$ shown in (b) and the decoupling ratio $\mathcal{R}_{1,2}$ in (c). The extent to which the decoupling and recoupling works is reflected by the temporal growth of the entanglement entropy, shown stroboscopically in (d) for two spins initially in the $|\uparrow\rangle \otimes |\downarrow\rangle$ state (corresponding parameter regimes indicated by crosses in (c)).

We now discuss the central result of our work, recoupling via the NVs acting as local actuators. As reflected by $\mathcal{R}_{j,j'}$ in Fig. 3 (c) and the entanglement entropy growth in Fig. 3 (d), the NV, acting as a local actuator several nanometers from the nuclear spins, can disrupt the protocol in the sensitive regime and recouple the spin interaction to almost the original strength [47]. This is again corroborated by

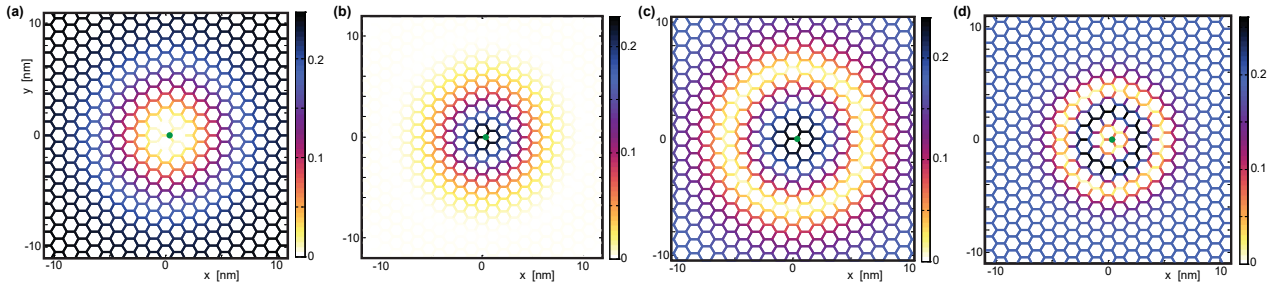

FIG. 4. **Selective decoupling in hexagonal spin networks:** Qualitatively different spatial coupling topologies can be created within our protocol in conjunction with a local actuator (e.g. an NV center) located several nanometers (between 5.7nm and 10nm here) below a ^{13}C hexagonal spin lattice. The decoupling ratio $\mathcal{R}_{j,j'}$ (directly proportional to the effective interaction strength $||\overline{\mathcal{H}}_{j,j'}||$) for all nearest neighbor spin pairs is shown in color-coded form with the spins located at the respective nodes. Depending on the chosen parameters, the decoupling protocol has a different length scale which can be exploited to give rise to different coupling structures. For instance, one can create a *non-interacting patch* (**a**) within an otherwise interacting network or vice versa, create a small *interacting cluster* in an otherwise essentially non-interacting lattice as shown in (**b**). Moreover, the parameters can be tuned to separate off an *interacting patch* shown in (**c**), or create an effective *1D ring-like lattice topology*, shown in (**d**). For all subfigures $N_c = 1$, the NV-center is activated throughout the wait period τ (amplifying the effect on $\overline{\mathcal{H}}$) and located at $(x = 0.355\text{nm}, y = 0)$ (green circle) with variable depth z and the ^{13}C spins are located on a regular hexagonal sublattice with lattice constant $a_{\text{lat}} = 5a_{\text{cc}}$, where $a_{\text{cc}} = 0.142nm$ is the carbon-carbon bond length and the lattice constant of graphene. We choose this sublattice configuration to obtain a system in a *weakly interacting regime*, i.e. allowing the true decoupling ratio to be obtained from a pairwise treatment of spins and avoid many-body effects. A relative agreement of 99.5% or more is found with a six spins cluster calculation (including the nearest neighboring spins). For detailed parameters see [42].

the rapid growth of the entanglement entropy (blue dots) in Fig. 3 (d) relative to the decoupled case (orange dots). The localized nature of the NVs breaks the translational symmetry of the inter-spin interaction, making the latter a function of the coordinates of both spins, as well as the NV positions. The resulting interaction form deviates from the typical $|\mathbf{r}-\mathbf{r}'|^{-3}$ dipolar interaction form. Furthermore, the structure of $\overline{\mathcal{H}}$ is fundamentally different: whereas $\mathcal{H}_{j,j'}$ is always of an XXZ-form in a suitably rotated basis, $\overline{\mathcal{H}}_{j,j'}$ can be of a more general form. If the rotation axis of $\mathcal{U}_{\text{el}}$ lies on the magic axis, we always find decoupling [42], i.e. $\mathcal{S}_{j,j'} \approx 0$.

Next, we demonstrate selective decoupling on a hexagonal sublattice of nuclear spins, as realized in graphene or 2D HBN above a shallow NV in diamond in a recent single spin NMR experiment [20]. In this system, we demonstrate the selective local decoupling of a spin cluster, as well as the creation of a locally coupled subnetwork, which is decoupled from the remaining network. Both constitute important tools in realizing locally addressable quantum memories. To achieve this, we pick a spin pair j, j', for which we optimize the decoupling procedure. First, we pick an approximate τ_1, which sets the sensitivity (see Fig. 2(b)) and the number of required concatenations of the protocol. Picking a decoupling peak in the τ_a, τ_b parameter space and using initial values close to the true minimum, we optimize $\mathcal{R}_{j,j'}$ in the presence of the other spins. This sets the timings for the full network and thus fully determines $\overline{\mathcal{H}}$. Within this numerically exact network simulation, the decoupling works very well, often leading to $\mathcal{R} < 10^{-10}$ for the optimized pair. In Fig. 4 the decoupling ratio between all nearest neighbor pairs are shown for spins arranged on a sublattice of a graphene sheet. By carefully choosing the timings and NV position relative to the decoupling pair j, j' and the lattice symmetry points, various scenarios are possible: a local *non-interacting patch* can be *burned* into the lattice (Fig. 4 (a)), useful, for example, for a temporary quantum memory. Other decoupling topologies are also possible: for instance we can create small interacting patches (Fig. 4 (b,c)) or ring-like topologies (Fig. 4 (d)), decoupled from the rest of the lattice [48].

In summary, we have introduced a versatile method for selective Hamiltonian engineering of dipolar spin networks using local actuator control. It should be noted that one can easily switch between two different effective Hamiltonian regimes as those shown in Fig. 4 (a) and (b) during a single experimental run by simply changing the protocol timings [49]. Our method relies on a modified version of magic angle spinning, but carried out by global fields in conjunction with spin actuators that provide a sensitive tool for decoupling or recoupling interactions with tunable range of action. This technique presents a compelling strategy for nanoscale Hamiltonian engineering and opens the path for quantum simulators constructed out of dipolar networks. We envision immediate applications in diamond based architectures [19, 20], and in the emerging field of molecular magnets [26, 27, 29], where highly coherent electronic spins such as vanadium in inorganic molecular complexes can serve as actuators of surrounding nuclear spins in order to control, decouple and re-couple them; opening pathways for the use of such systems in quantum simulation.

We gratefully thank A. Pines for insightful conversations. U.B. and D.P. acknowledge support by the Air Force Office of Scientific Research under Award No.FA2386-16-1-4041. P.C. acknowledges support from NSF under PHY1734011 and PHY1415345, and ARO under W911NF-15-1-0548.

* These authors contributed equally to this work.
† ashokaj@berkeley.edu

[1] R. Blatt and C. F. Roos, Nat Phys **8**, 277 (2012).
[2] I. Bloch, J. Dalibard, and S. Nascimbène, Nature Physics **8**, 267 (2012).
[3] A. Aspuru-Guzik and P. Walther, Nature Physics **8**, 285 (2012).
[4] A. A. Houck, H. E. Türeci, and J. Koch, Nature Physics **8**, 292 (2012).
[5] V. Giovannetti, S. Lloyd, and L. Maccone, Nat. Photon **5**, 222 (2011).
[6] S. Schirmer, in *Lagrangian and Hamiltonian Methods for Nonlinear Control 2006*, Lecture Notes in Control and Information Sciences, Vol. 366 (Springer, 2007) pp. 293–304.
[7] F. Verstraete, M. M. Wolf, and J. Ignacio Cirac, Nat Phys **5**, 633 (2009).
[8] B. Kraus, H. P. Büchler, S. Diehl, A. Kantian, A. Micheli, and P. Zoller, Phys. Rev. A **78**, 042307 (2008).
[9] A. Ajoy and P. Cappellaro, Phys. Rev. Lett. **110**, 220503 (2013).
[10] R. P. Feynman, Inter. J. Th. Phys. **21**, 467 (1982).
[11] S. Lloyd, Science **273**, 1073 (1996).
[12] J. I. Cirac and P. Zoller, Nature Physics **8**, 264 (2012).
[13] L. Viola and S. Lloyd, Phys. Rev. A **58**, 2733 (1998).
[14] E. R. Andrew, A. Bradbury, and R. G. Eades, Nature (London) **182**, 1659 (1958).
[15] M. Lee and W. Goldburg, Phys. Rev. A **140**, 1261 (1965).
[16] M. Duer, *Introduction to Solid-State NMR Spectroscopy* (John Wiley & Sons, 2004).
[17] A. Pines and J. Waugh, Journal of Magnetic Resonance **8**, 354 (1972).
[18] A. Pines and L. Emsley, *Lectures on Pulsed NMR* (Proceedings of International School of Physics (Fermi Lectures), 1992).
[19] J. Cai, A. Retzker, F. Jelezko, and M. B. Plenio, Nature Physics **9**, 168 (2013).
[20] I. Lovchinsky, J. Sanchez-Yamagishi, E. Urbach, S. Choi, S. Fang, T. Andersen, K. Watanabe, T. Taniguchi, A. Bylinskii, E. Kaxiras, *et al.*, Science **355**, 503 (2017).
[21] S. Choi, N. Y. Yao, and M. D. Lukin, (2017), arXiv:1703.09808.
[22] U. Boscain and P. Mason, Journal of Mathematical Physics **47**, 062101 (2006).
[23] N. Khaneja, Phys. Rev. A **76**, 032326 (2007).
[24] T. W. Borneman, C. E. Granade, and D. G. Cory, Phys. Rev. Lett. **108**, 140502 (2012).
[25] T. H. Taminiau, J. J. T. Wagenaar, T. van der Sar, F. Jelezko, V. V. Dobrovitski, and R. Hanson, Phys. Rev. Lett. **109**, 137602 (2012).
[26] M. Atzori, E. Morra, L. Tesi, A. Albino, M. Chiesa, L. Sorace, and R. Sessoli, Journal of the American Chemical Society **138**, 11234 (2016).
[27] C.-J. Yu, M. J. Graham, J. M. Zadrozny, J. Niklas, M. D. Krzyaniak, M. R. Wasielewski, O. G. Poluektov, and D. E. Freedman, Journal of the American Chemical Society **138**, 14678 (2016).
[28] K. S. Pedersen, A.-M. Ariciu, S. McAdams, H. Weihe, J. Bendix, F. Tuna, and S. Piligkos, Journal of the American Chemical Society **138**, 5801 (2016).
[29] R. Hussain, G. Allodi, A. Chiesa, E. Garlatti, D. Mitcov, A. Konstantatos, K. S. Pedersen, R. De Renzi, S. Piligkos, and S. Carretta, Journal of the American Chemical Society (2018).
[30] F. Jelezko and J. Wrachtrup, Physica Status Solidi (A) **203**, 3207 (2006).
[31] A. Sushkov, I. Lovchinsky, N. Chisholm, R. Walsworth, H. Park, and M. Lukin, Physical review letters **113**, 197601 (2014).
[32] A. Ajoy, U. Bissbort, M. Lukin, R. Walsworth, and P. Cappellaro, Phys. Rev. X **5**, 011001 (2015).
[33] F. Shi, Q. Zhang, P. Wang, H. Sun, J. Wang, X. Rong, M. Chen, C. Ju, F. Reinhard, H. Chen, *et al.*, Science **347**, 1135 (2015).
[34] I. Lovchinsky, A. Sushkov, E. Urbach, N. de Leon, S. Choi, K. De Greve, R. Evans, R. Gertner, E. Bersin, C. Müller, *et al.*, Science **351**, 836 (2016).
[35] Z.-Y. Wang, J. F. Haase, J. Casanova, and M. B. Plenio, Physical Review B **93**, 174104 (2016).
[36] D. Burgarth and A. Ajoy, Phys. Rev. Lett. **119**, 030402 (2017).
[37] R. Nandkishore and D. A. Huse, Annu. Rev. Condens. Matter Phys. **6**, 15 (2015).
[38] C. L. Degen, M. Poggio, H. J. Mamin, C. T. Rettner, and D. Rugar, Proc. Nat. Acad. Sc. **106**, 1313 (2009).
[39] H. J. Mamin, C. T. Rettner, M. H. Sherwood, L. Gao, and D. Rugar, App. Phys. Lett. **100**, 013102 (2012).
[40] This neglects terms which change the total energy $\propto s_z = I_z^{(1)} + I_z^{(2)}$, justified in a strong background magnetic field $\mathbf{B}_0$.
[41] The extension to multiple spins is simply given by taking the direct product of the rotation operators for each spin.
[42] See supplementary online material.
[43] A. Ajoy, Y.-X. Liu, K. Saha, L. Marseglia, J.-C. Jaskula, U. Bissbort, and P. Cappellaro, Proceedings of the National Academy of Sciences **114**, 2149 (2017).
[44] Given that the rotation axis of $\mathcal{U}^{(N_c)}$ is sufficiently large $\theta_{\rm tilt}^{(N_c)} \in [\theta_{\rm M}/2, \theta_{\rm M}]$, the topological structure of the resulting flip and tilt angle of $\mathcal{U}_{\rm tot}$ guarantees that suitable values of τ_a and τ_b always exist [42] to reach exactly the magic angle and a fractional flip angle of $2\pi/m$.
[45] U. Haeberlen, J. E. Jr, and J. Waugh, Journal of Chemical Physics **55**, 53 (1971).
[46] Nine orders of magnitude or more can be reached when optimizing around other decoupling peaks.
[47] We emphasize that the strong recoupling occurs despite the NVs' magnetic field contribution being three orders of magnitude smaller than $\mathbf{B}_0$.
[48] These result are obtained for ^{13}C nuclear spins spaced at a large distance on a graphene sublattice, where the system is weakly interacting. By choosing a smaller inter-spin distance, the system can be brought into a strongly interacting regime, where the effective interaction between a given pair of spins also strongly depends on the neighboring spins, leading to a highly non-trivial system beyond the scope of this work.
[49] Effective additional, yet relatively small, interactions (e.g. two or three spin terms) may also arise in $\mathcal{H}$, and these are also well captured and explained in higher orders of the Magnus expansion [42].